Closed-Loop Stall Control on a Morphing Airfoil Using Hot-Film Sensors and DBD Actuators

Jonathan Poggie,* Carl P. Tilmann, and Peter M. Flick
Air Force Research Laboratory, WPAFB OH

Joseph S. Silkey and Bradley A. Osborne
Boeing Integrated Defense Systems, St. Louis MO

Gregory Ervin and Dragan Maric
FlexSys, Ann Arbor MI

Siva Mangalam and Arun Mangalam
Tao of Systems Integration, Hampton VA

A closed-loop, stall sense and control system was demonstrated on a morphing airfoil. The FlexSys, Inc. Mission Adaptive Compliant Wing (MACW) was modified to accept a Boeing Co. dielectric barrier discharge (DBD) actuator panel in a location immediately upstream of the trailing-edge morphing flap, and hot-film sensors were installed on the model surface. A signal analysis algorithm, developed by Tao Systems, Inc, was applied to the hot-film signals to detect separation and trigger activation of the DBD actuators. The system was successfully demonstrated in the AFRL SARL wind tunnel facility, and an improvement in lift of about 10% was observed at Mach 0.05 (chord Reynolds number 9×10^5) under closed-loop control and a turbulent boundary layer state. Actuator effectiveness was demonstrated up to Mach 0.1, but must be extended to Mach 0.2–0.3 to enable a practical stall control system for takeoff and approach of large aircraft.

I. Introduction

This paper reports the results of a program to demonstrate a closed-loop, stall sense and control system, integrating the technologies of plasma flow control, morphing structures, and instantaneous sensing of flow topology. The program involved a multi-disciplinary partnership of government and industry. FlexSys, Inc. provided the basic test article, a wing with a morphing flap that permits continuous shape change to maximize aerodynamic efficiency under different flight conditions.[1–3] Tao Systems, Inc. provided a system that can directly sense the instantaneous location of separation and reattachment using an array of flush-mounted hot-film anemometers and unique signal-processing algorithms.[4,5] The Boeing Co. provided a flush-mounted panel of dielectric barrier discharge plasma actuators to mitigate flow separation.[6] The Air Force Research Laboratory developed the system concept, and provided the wind tunnel test facilities.

Although a number of studies of closed-loop control have been carried out for canonical configurations, such as cylinder flows,[7] there have been relatively few previous studies of closed-loop stall control systems for large-scale airfoil configurations. The existing studies have used surface pressure sensors to detect separation, and have employed either synthetic jet actuators[8] or DBD actuators for stall mitigation.[9] Similarly, DBD actuators are a topic of intensive international research,[10–14] but there has been a lack of attention to the application of DBD actuators to large-scale configurations. Published studies on relatively large-scale configurations have included a study[15] of DBD-based flight control of the USAF/Boeing 1303 UCAV configuration at a chord Reynolds number of 4×10^5, and flight testing on a sailplane.[16]

The present program differs from these previous studies in that the hot-film sensors provide a direct indication of flow separation (unlike pressure measurements), and that the system has been demonstrated on a relatively large-scale configuration suitable for SensorCraft[2] applications. The program had two main objectives:

*Cleared for public release, distribution unlimited (88ABW-2009-4976).

1. Demonstrate that an array of flush-mounted hot-film anemometers can determine the instantaneous flow state by tracking the location of separation and reattachment. In particular, quantify the relationship between leading-edge stagnation line location and lift, flap deflection, and angle-of-attack.

2. Demonstrate closed-loop control of airfoil stall: detect the onset of separation with surface hot-film sensors and use their output to trigger plasma actuators to reattach the flow.

The program successfully achieved both objectives. Real-time stagnation line location measurement was demonstrated, and stagnation location was found to be a nearly linear function of angle-of-attack and flap deflection. Closed-loop control of separation over the trailing-edge flap was achieved, improving lift by about 10% at Mach 0.05.

II. Experimental Procedure

The experiments were carried out in October/November 2008, in the Phillip P. Antonatos Subsonic Aerodynamics Research Laboratory (SARL) at Wright-Patterson Air Force Base. The SARL facility is a high contraction ratio, open-circuit wind tunnel that can provide flow speeds in the range of Mach 0.05-0.5. The test section is 15 ft (4.57 m) long, with a 63.1 ft^2 (5.86 m^2), octagonal cross-section. For the present research, testing was carried out in the Mach number range 0.05-0.10, for corresponding Reynolds numbers based on airfoil chord of 0.9×10^6–1.7×10^6.

Two views of the model installed in the wind tunnel test section are shown in Fig. 1. Figure 1a shows the view looking downstream toward the wind tunnel fan. The model is visible on top of its support pedestal, with the power cabling conduit extending above. For an angle-of-attack of 12 deg, the combination of the airfoil and associated equipment occupied a cross-sectional area of 4.53 ft^2 (0.42 m^2), for total blockage of 7.2%. The wind tunnel facility provided a traversable wake-rake probe system, which is visible in the background. Figure 1b shows the view looking upstream, showing the plasma actuator panel mounted on the suction side of the airfoil, and the hot-film arrays affixed to the surface.

A. Wind Tunnel Model

The basic test article was the FlexSys, Inc. Mission Adaptive Compliant Wing (MACW), which has been previously tested in the SARL wind tunnel facility, and has been flight tested, mounted underneath the Scaled Composites, Inc. White Knight aircraft.[1–3] The model consists of a natural laminar flow (NLF) airfoil with a trailing-edge morphing flap. The wing has a 50 in (1.270 m) span and a 30 in (0.762 m) chord, with elliptical endplates (45 in x 24 in or 1.143 m x 0.610 m) to help minimize three-dimensional effects (see Figs. 1-2).

The rear 30% of the airfoil is a morphing, trailing-edge flap, capable of continuous shape change for flap deflections in the range of −10 deg to +10 deg. Under remote control, two servomotors mounted inside the wing are capable of driving the flap deflection at 30 deg/s, in an unloaded condition.

The main body of the model was constructed of aluminum, and the morphing flap was made of aluminum and polymer composites. The lower surface of the flap contains a composite-reinforced, silicon elastomer panel that expands and contracts to allow the structure to change shape.

Model angle of attack can be varied within a 10 deg arc by an onboard motor, subject to an offset determined by interchangeable mounting plates. The available mounting plates provided five ranges of angle-of-attack: −3 deg to 7 deg, 2–12 deg, 7–17 deg, and 12–22 deg. Most of the flow control tests were carried out in the 12–22 deg range.

Figure 2 identifies the primary elements of the test article and their locations on the model. The model has static pressure taps on its upper and lower surfaces; the pressure data were integrated to obtain lift and pitching moment. Plumbing for the pressure taps was routed out through the pedestal.

Dantec hot-film sensors were installed flush with the model surface to determine laminar vs. turbulent boundary layer state at 25%, 35%, and 45% chord. These are labeled 'Transition Hot Films' in Fig. 2. Although the natural laminar flow airfoil design is theoretically capable of achieving 65% chord laminar flow on the suction side and 90% chord laminar flow on the pressure side, this level of performance was not obtained in the present experiments, most likely because of relatively high freestream turbulence levels. Transition was detected at 45% chord at 8 deg angle-of-attack, and had progressed upstream of the 25% chord station by 12 deg angle-of-attack. Thus all the flow control experiments were carried out for a turbulent boundary layer state.

B. Stagnation Line Sensing Technique

Arrays of hot-film sensors, or constant-overheat anemometers, were fabricated in 0.006 in (0.15 mm) flexible sheets that were affixed to the airfoil surface. A Parylene coating was used to mitigate possible corrosion from the plasma introduced into the flow by the DBD actuators. The sensors were run in constant overheat mode, and responded to shear stress at the airfoil surface. They are labeled COA in Figs. 1-2. Arrays of sensors were affixed at various locations on the model to monitor the structure of the flow: the leading edge array sensed stagnation line location; an array on the flap downstream of the actuator sensed flap separation state; and supplemental arrays located on the inboard portion of the model tracked separation movement across the plasma actuator panel. The system has high signal-to-noise ratio and bandwidth (greater than 10 kHz).

Real-time signal processing of data from an array of hot-film sensors can be used to deduce information about the flow around a body, such as the location of stagnation lines, laminar-turbulent transition, flow separation, and shock waves.[4,5] In particular, these sensors can identify critical points in the surface shear stress vector field, points where the vector magnitude is zero, vector direction is undefined, and local flow topology changes.[17] A variety of criteria can be used to detect a flow critical point using a hot-film array: minimum shear stress, signal phase reversal across the critical point, and signal frequency doubling at the critical point. Interpolation can be used to discern the position of critical points between sensors.

With the critical points identified, much of the flow structure can be inferred, since the structure of the inviscid outer flow is dictated by the airfoil geometry and shape of the stream-surface bounding the separation bubble. Once an approximate specification of this outer flow structure is available, it is possible to estimate flow quantities such as lift and pitching moment. Thus a stagnation line sensor can be used to measure lift and pitching moment, and this idea was investigated in the present study.

During closed-loop control testing, the plasma actuators were triggered when the hot-film signal exceeded a threshold shear stress that occurred when the separation line was located over the plasma actuator panel.

C. Plasma Actuators

Dielectric barrier discharge (DBD) plasma actuators consist of two high-voltage electrodes separated by a dielectric (insulating) layer. A varying applied voltage leads to transient formation of space charge and strong electric fields, creating an electrical body force on the flow. With an appropriate arrangement of the electrodes, this force generates a streamwise wall-jet flow, with a velocity on the order of a few meters per second. These actuators can be useful for controlling low-speed flows, with the advantages of conformal mounting, a low profile when not in use, no moving parts, and relatively low power requirements (on the order of Watts for a typical panel). Although similar devices based on the 'ion wind' effect had been considered previously,[18,19] actuators specifically based on dielectric barrier discharges were first introduced as flow control devices in the mid-1990s.[20] They are currently the topic of intensive international research.[10–14]

The wind tunnel model was modified to include a plasma actuator panel located upstream of the flap. This panel was designed to mount flush with the upper-surface mold line of the airfoil. The footprint of the actuators was optimized to provide separation control over a large portion of the trailing edge. The actuators were integrated into 32.0 in x 5.0 in (0.813 m x 0.127 m) removable panels that fit into a machined cutout on the upper surface of the model, forward of the compliant flap between 49% and 66% chord (see Fig. 2). The buried electrode chord dimension was 3.0 in (76 mm). A 1.0 in (25 mm) surface electrode clearance from the model electrical grounds was maintained to prevent arcing at anticipated actuation voltages. The spanwise extent of the electrodes was 30.0 in (0.762 m, or 60% of span).

Two general types of DBD actuators were fabricated: thick Teflon actuators and thin Kapton actuators. The thick actuator design used a 0.25 in (6.4 mm) thick, machined Teflon dielectric layer, with various additional dielectric coatings. The thin Kapton actuator designs employed a 0.02 in (0.5 mm) thick dielectric layer. For both types of actuator, thin copper electrodes were mounted on the upper and lower surfaces of the dielectric.

Table 1 lists the types of actuator tested, and corresponding photos are shown in Figs. 3-4. Configuration A consisted of a 0.25 in thick Teflon dielectric layer with a spanwise 30.0 in by 0.5 in surface electrode. Configuration B was similar, but 3.0 in (76 mm) long, streamwise 'finger' electrodes were added with a 3.0 in (76 mm) spacing on center. Configuration C was based on Configuration B, but with a 0.014 in layer of Kapton added to the dielectric layer. Configuration D consisted of a 0.02 in (0.5 mm) thick Kapton layer affixed to a stereolithography blank. For this case, the streamwise finger electrodes were spaced 2.0 in

(51 mm) on center.

Configuration E showed the best performance in mitigating flap separation, and is illustrated in Fig. 4. This actuator was a variant of Configuration C, in which a 0.02 in (0.5 mm) thick layer of Kapton and Teflon was bonded on the top of the 0.25 in (6.4 mm) thick Teflon insert.

In the flow control experiments, the actuators were tested over a range of 5-18 kV_{rms} (14-50 kV_{p-p}), primarily with a sinousoidal 1.5-2.5 kHz driving waveform.

D. Electromagnetic Interference Testing

Bench tests of components sensitive to electromagnetic interference were conducted prior to the wind tunnel tests to develop and verify operational compatibility. The components of concern were the morphing flap motor / controller, electronic pressure sensing module, angle-of-attack positioner, and surface hot films. All electromagnetic interference issues were resolved prior to testing. In particular, negligible interference was observed between the plasma actuators and the hot-film sensors.

To further mitigate potential electromagnetic interference, the electronic scanned pressure module for the surface pressure measurements was located outside the model, and power lines were routed to avoid proximity to internal electrical components. The conduit for supplying power to the plasma actuators is visible at the top of each photo in Fig. 1. All power leads were inserted inside flexible PVC tubing, and disk inserts inside the conduit held the power leads apart. All instrumentation cabling was routed out of the bottom of the pedestal mount.

III. Results

The test program was carried out in three phases. First, tests were carried out to demonstrate that the arrays of flush-mounted hot-film sensors could determine the instantaneous flow state by tracking the location of separation and reattachment. Next, open-loop control experiments were carried out with the DBD plasma actuators to demonstrate that they could mitigate separation for these test conditions. Finally, tests were carried out to demonstrate closed-loop control of airfoil stall by detecting the onset of separation with hot-film anemometers, and using their output to trigger plasma actuators to reattach the flow.

A. Stagnation Line Mapping

The first phase of testing addressed real-time stagnation line tracking with the hot-film arrays. Stagnation line location was determined through the hot-film array mounted on the leading edge, and lift was computed by integrating the surface pressure distribution.

Figure 5a shows lift as a function of angle-of-attack and flap deflection for a Mach 0.05 flow condition. As expected, lift varies nearly linearly with both angle-of-attack and flap deflection angle, with a roll-off at large angles. The corresponding stagnation line location, determined using the leading edge hot-film array, is shown in Fig. 5b. The stagnation line location is also seen to be a nearly linear function of angle-of-attack and flap deflection. For increasing angle-of-attack, or increasing flap deflection, circulation increases, and the stagnation line moves toward / along the pressure side of the airfoil (positive stagnation line direction in the figure).

Since lift and stagnation line location are both nearly linear functions of angle-of-attack, it should be possible to correlate lift with stagnation location, and use the hot-film sensors to measure lift. This idea is illustrated in Fig. 5c, which shows lift as a function of stagnation line location and flap deflection. For a fixed airfoil geometry (flap deflection), lift is seen to be a monotonic function of stagnation line location, indicating that the array of leading edge sensors could be used as a lift sensing system.

At higher angles-of-attack the stagnation line moved beyond the installed range of the array of hot-film sensors, rendering precise measurement of the stagnation location for conditions beyond 13 deg angle-of-attack impossible with the present sensor installation. This limitation precluded use of the leading-edge stagnation point as a feedback signal for flow control, because the regime of interest for control was in the 13–17 deg range, where the stagnation line could not be precisely resolved. Thus, the closed-loop control experiments (discussed later in this paper) used the sensors on the flap as the control input.

The other arrays of hot-film sensors were used to map out the locations of separation and reattachment. An additional test series was carried out to map separation location using a blank insert with hot films in

place of the actuator panel. Light yarn tufts were used as a verification check of the measured separation location.

Pretest CFD analysis predicted a separation line on the plasma actuator panel in the 9–15 deg angle-of-attack range, and stall was predicted to occur by 20 deg angle-of-attack. The test data revealed that separation actually occurred at angles-of-attack between 12 deg and 17 deg, about 3 deg higher than predicted by the two-dimensional computations. Complete stall could not be achieved with the baseline airfoil configuration, which was restricted to a maximum angle-of-attack of 22 deg. The discrepancy between computation and experiment is probably due to three-dimensionality in the experimental flow related to undersized model endplates.

B. Flow Control Effectiveness

The effectiveness of plasma flow control was evaluated using several different actuators at Mach numbers of 0.05–0.10, angles-of-attack of 7–22 deg, and flap deflections of -10 deg to 10 deg. A list of all the actuator configurations tested is given in Table 1, and corresponding pictures are given in Figs. 3-4. All the flow control experiments were carried out for a turbulent boundary layer state, as indicated by the hot-film sensors upstream of the actuator panel.

Driving waveforms and input voltage amplitudes were varied to assess their effect on flow control for various conditions. A limited study of the effect of input signal modulation was done at 20% duty cycle for modulation frequencies between 28-234 Hz, in the vicinity of $fL/V_\infty = 1$ for the separation bubble. A continuous waveform was the most effective input signal at all evaluated conditions, so only those results are presented here. Further exploration of signal modulation strategies is warranted, however, and a broader range of duty cycles needs to be examined in particular.

Actuator Configurations A and B were found to be ineffective, and were not pursued further in the experiments. The single element spanwise electrode arrangement (Configuration A) was found to be much less effective than the other actuator configurations, probably because the separation location was considerably downstream of the actuation location for all the cases tested. The finger electrodes used with the other actuator configurations impose control over a broader streamwise range, so they are effective for a broader range of separation line locations. The thick Teflon actuators without an additional dielectric overlay (Configuration B) suffered from burn-through at relatively low voltages, so it was not possible to make a clear comparison between the baseline thick and thin actuator designs. The remainder of this discussion will focus on Configurations C, D, and E, which were resistant to burn-through, and relatively effective for flow control.

Figure 6 illustrates flow control performance for Configuration C, a 0.264 in (6.71 mm) thick Teflon-Kapton actuator with multiple, streamwise finger electrodes. Figure 6a shows the change in lift, as a function of angle-of-attack, for different actuation voltage levels. Control effectiveness is seen to initially increase with angle of attack, then drop off. This behavior corresponds to the separation line moving onto the actuator panel, increasing control effectiveness, then moving upstream past the panel, diminishing effectiveness.

Lift was determined by integrating the measured pressure distribution over the airfoil surface. A block of pressure taps had to be removed to install the actuator panel, so interpolation was used to estimate pressures across this missing span. Thus, the change in sectional lift coefficient is probably underestimated here. Further, the fact that the actuation was imposed on only 60% of the model span tends to reduce the control effectiveness from what could be achieved for a condition with uniform spanwise conditions.

The effect of changes in voltage applied across the actuator is also illustrated in Fig. 6a. Actuator authority is seen to increase with increased voltage. In all cases the upper bound on actuator performance was actuator failure through burn-through, which was dictated mainly by dielectric material thickness, composition, and actuator construction technique.

For the case highlighted in Fig. 6a (15 deg angle-of-attack, 12.7 kV_{rms} input voltage), the lift is seen to improve by about 10% when control is applied. Figure 6b shows the corresponding surface pressure distributions for this case, and Fig. 6c shows the corresponding wake profiles. Reduced pressures (increased suction) are observed over most of the suction side of the airfoil, with a slight increase in pressure on the opposite surface. The wake rake survey shows that the wake is deflected approximately 5 in (127 mm) toward the pressure side of the airfoil with control applied.

Lift and moment coefficients for the case of a 12.7 kV_{rms} input voltage applied to Configuration E are shown in Fig. 7 as a function of angle of attack and Mach number. The results for Mach 0.05 are shown in Figs. 7a-b. The effect of the plasma actuators is to increase the magnitude of both the lift and moment coefficients, with the effect increasing with angle-of-attack over the range tested. The corresponding plots

for Mach 0.10 are shown in Figs. 7c-d, and illustrate the diminishing effectiveness of control with increasing Mach number.

The influence of actuator voltage and freestream Mach number on lift is shown in more detail in Fig. 8. The results for actuator Configuration C are shown in Fig. 8a, and for Configuration D in Fig. 8b. The higher voltage / thicker dielectric actuators showed the greatest effectiveness. The 0.264 in (6.71 mm) thick Teflon actuator (Configuration C) had almost twice the lift increment of the 0.02 in (0.5 mm) thick Kapton actuator (Configuration D). Control effectiveness decreased with increasing Mach number, roughly correlating with dynamic pressure ($\propto 1/V_\infty^2$), which suggests a momentum scaling.

Unfortunately, the full potential of the thick actuator could not be demonstrated because of failure of the dielectric barrier through burn-through. Data repeatability was hampered by the oscillatory nature of the separated flow, as is evident with the data point scatter in the figure. A suitable averaging procedure might improve the consistency of the results.

Plots of shear stress versus angle-of-attack are shown in Fig. 9 for Configuration E. The measured shear values on the suction side of the flap decrease as angle-of-attack is increased because the separation line is moving upstream from the trailing edge (Figs. 9a and 9c). The measured shear values on the pressure side of the leading edge (Figs. 9b and 9d) increase as angle-of-attack is increased because the local flow velocity increases with circulation.

The effects of actuation are readily evident in the shear stress; in all cases the shear stress increases with the actuators on. The effectiveness of control is strongly influenced by the location of the actuators relative to the location of separation. For the case shown Fig. 9a, the separation line is downstream of the actuator for low angles of attack. The actuator effectiveness increases with angle-of-attack as the separation line moves upstream towards the actuator. Control effectiveness peaks at 15 deg, when the separation location closely matches the actuator location, then decreases as the separation line moves progressively upstream of the actuator.

C. Closed Loop Flow Control Demonstration

Closed loop flow control was demonstrated using an automated controller to trigger the plasma actuators (Configuration E) when the flap hot-film sensors indicated that separation had moved onto the actuator panel. Separation was sensed with the hot-film sensors on the trailing-edge flap, located downstream of the actuators. The effectiveness of control was observed with the flap and leading edge hot-film sensors, as well as through static pressure measurements and the corresponding integrated lift changes.

The following experimental procedure was employed:

1. Determine the output of the flap hot-film array that corresponds to a separation line location on the plasma actuator panel.
2. Set the corresponding shear trigger threshold in the control software, and engage the controller.
3. Start the model at a pre-separation angle-of-attack (12 deg), with fixed flap setting of +10 deg.
4. Begin the model angle-of-attack sweep.
5. Wait for the controller to automatically trigger DBD actuation when the shear level reaches the preset value.
6. Stop the model angle-of-attack sweep.
7. Record actuation-on data (pressures, shear stress).
8. Deactivate the DBD actuator, and record actuation-off data.

The control system is shown in Fig. 10. The control system latches when flap shear stress reaches the predetermined set point. The flap shear stress signal was calibrated to separation location prior to the flow control demonstration to determine the required signal threshold. (See Figs. 9a, 11a.) The output modulation gate signal was sent to the power supply waveform generator to drive the actuator high-voltage circuits. The actuation waveform parameters, such as carrier and modulation frequency, amplitude, duty cycle, and shape were programmable and could be computed dynamically. The controller provided real-time signal monitoring and spectral analysis, enabling the operator to find receptive modulation frequencies.

Shear-stress time-histories are shown for one demonstration in Fig. 11. The shear stress signal was not calibrated to physical units, but signal magnitudes are comparable between sensors. It can be seen that leading-edge shear is much higher than trailing-edge shear. The green dots represent raw shear stress data and the blue line represents a median filter. The scatter is not electronic, but rather due in large part to flow fluctuations resulting from low-speed wind tunnel operation. (Flow quality in the SARL facility is somewhat degraded at this low end of its speed range, Mach 0.05.)

The vertical red dotted line on the shear plots indicates that the control system turned the plasma actuator on at 17 deg angle-of-attack. The shear on the suction side of the flap jumps up significantly as flow attaches. For this Mach 0.05 case, the actuation at 17 deg angle-of-attack provides about the same effect on lift as a change of one degree angle-of-attack. The trailing edge shear data display oscillations with a period on the order of 10–15 s, probably corresponding to oscillation of the separation bubble back and forth across the hot-film sensor.

IV. Summary and Conclusions

This paper reports on a program to demonstrate a closed-loop, stall sense and control system, integrating the technologies of plasma flow control, morphing structures, and instantaneous sensing of flow topology. Under this program, the Mission Adaptive Compliant Wing was modified to accept a dielectric barrier discharge plasma actuator panel in a location immediately upstream of the trailing-edge morphing flap. Hot-film sensors were installed on the model surface to determine the location of separation. The hot-film data were used to trigger activation of the dielectric barrier discharge actuators for closed-loop flow control.

The test article was installed in the SARL wind tunnel facility at Wright-Patterson Air Force Base, and tests were conducted to map separation locations and identify boundary layer state as a function of angle-of-attack and Mach number. Lift was calculated by integrating surface pressure data, and wake momentum deficit was investigated with a wake rake probe system.

The leading-edge stagnation line was tracked in real time by the surface hot-film system, as the model underwent angle-of-attack sweeps, and was found to be a monotonic function of lift. Flow control testing was conducted with the plasma actuators over a range of Mach numbers of 0.05–0.1, chord Reynolds numbers of 0.9×10^6–1.7×10^6, angles-of-attack of 7–22 deg, and flap deflections from -10 deg to $+10$ deg.

Several plasma actuator designs were tested. The best performing actuator was found to be a 0.25 in (6.4 mm) thick Teflon dielectric with a 0.02 in (0.5 mm) thick layer of Kapton and Teflon bonded on the top of the Teflon. Generally, higher operating voltage improved performance. The thin Kapton actuator design increased effectiveness with increased voltage over the 7-9 kV_{rms} range, and the thick Teflon actuator design increased effectiveness with increased voltage over the 12-18 kV_{rms} range.

Flow control was most effective when the model angle-of-attack was in the 13–17 deg range, which corresponded to a separation location at the middle of the plasma actuator. Actuation was not as effective when the actuator was upstream or downstream of separation. Interestingly, actuation downstream of separation caused a net lift loss in some cases. The effect of actuation was insensitive to flap deflections in the -10 deg to $+10$ deg deflection range. The improvement decayed with Mach number increase, roughly in inverse proportion to the dynamic pressure.

The closed-loop flow control demonstration at Mach 0.05 achieved an improvement in section lift coefficient of about 10%. Control was triggered by flap shear sensors, and the effects of control were observed through flap and leading edge hot-film sensors as well as static pressure measurements.

Future work should focus on developing robust, high-authority actuators that can control flap separation and mitigate full stall at airspeeds up to Mach 0.2–0.3, corresponding to takeoff and approach speeds for large aircraft. Larger flap deflection angles, approaching 45 degrees, should also be tested. The recommended actuators include higher voltage AC actuators, and also the emerging nanosecond pulse actuators and arc-based actuators. Automated manufacturing methods should be used to improve reliability and operability.

Acknowledgments

This project was funded by the AFRL Air Vehicles Directorate, under contract F33615-00-D-3052-DO0091. Technical support was provided by the following individuals; AFRL: J. Hayes, K. King, R. Raber, F. Semmelmayer, and J. Tekell; Tao Systems: S. Parrish; Boeing: P. Boenitz, D. Cleland, T. Ganley, M. Rogers, C. Wilson, and M. Younger. Kapton and Teflon are registered trademarks of Dupont, Inc.

References

[1]Carter, D. L., Osborn, R. F., Hetrick, J. A., and Kota, S., "The Quest for Efficient Transonic Cruise," AIAA Paper 2007-7812, September 2007.

[2]Hetrick, J. A., Osborn, R. F., Kota, S., Flick, P. M., and Paul, D. B., "Flight Testing of Mission Adaptive Compliant Wing," AIAA Paper 2007-1709, April 2007.

[3]Youngren, H., "Multi-Point Design and Optimization of a Natural Laminar Flow Airfoil for a Mission Adaptive Compliant Wing," AIAA Paper 2008-293, January 2008.

[4]Mangalam, A. S., Mangalam, S. M., and Flick, P. M., "Unsteady Aerodynamic Observable for Gust Load Alleviation and Flutter Suppression," AIAA Paper 2008-7187, August 2008.

[5]Mangalam, A. S. and Davis, M. C., "Ground / Flight Correlation of Aerodynamic Loads with Structural Response," AIAA Paper 2009-881, January 2009.

[6]Sidorenko, A. A., Zanin, B. Y., Postnikov, B. V., Budovsky, A. D., Starikovskii, A. Y., Roupassov, D. V., Zavialov, I. N., Malmuth, N. D., Smereczniak, P., and Silkey, J. S., "Pulsed Discharge Actuators for Rectangular Wing Separation Control," AIAA Paper 2007-941, January 2007.

[7]Synder, B. L., Lewis, J. A., Cohen, K., Seaver, C. A., and McLaughlin, T., "Closed-Loop Plasma Active Control Technology (CLOPACT)," AIAA Paper 2007-108, January 2007.

[8]Becker, R., King, R., Petz, R., and Nitsche, W., "Adaptive Closed-Loop Separation Control on a High-Lift Configuration Using Extremum Seeking," *AIAA Journal*, Vol. 45, No. 6, 2007, pp. 1382–1392.

[9]Patel, M. P., Sowle, Z. H., Corke, T. C., and He, C., "Autonomous Sensing and Control of Wing Stall Using a Smart Plasma Slat," *Journal of Aircraft*, Vol. 44, No. 2, 2007, pp. 516–527.

[10]Forte, M., Jolibois, J., Pons, J., Moreau, E., Touchard, G., and Cazalens, M., "Optimization of a Dielectric Barrier Discharge Actuator by Stationary and Non-Stationary Measurements of the Induced Flow Velocity: Application to Airfoil Control," *Experiments in Fluids*, Vol. 43, No. 6, 2007, pp. 917–928.

[11]Santhanakrishnan, A. and Jacob, J. D., "Flow Control with Plasma Synthetic Jet Actuators," *Journal of Physics D: Applied Physics*, Vol. 40, No. 3, 2007, pp. 637–651.

[12]Enloe, C. L., McHarg, M. G., and McLaughlin, T. E., "Time-Correlated Force Production Measurements of the Dielectric Barrier Discharge Plasma Aerodynamic Actuator," *Journal of Applied Physics*, Vol. 103, No. 7, 2008, pp. 073302–1–073302–7.

[13]He, C., Corke, T. C., and Patel, M. P., "Plasma Flaps and Slats: An Application of Weakly Ionized Plasma Actuators," *Journal of Aircraft*, Vol. 46, No. 3, 2009, pp. 864–873.

[14]Little, J., Nishihara, M., Adamovich, I., and Samimy, M., "Separation Control from the Flap of a High-Lift Airfoil using DBD Actuators," AIAA Paper 2009-145, January 2009.

[15]Patel, M. P., Ng, T. T., Vasudevan, S., Corke, T. C., and He, C., "Plasma Actuators for Hingeless Aerodynamic Control of an Unmanned Air Vehicle," *Journal of Aircraft*, Vol. 44, No. 4, 2007, pp. 1264–1274.

[16]Sidorenko, A. A., Budovsky, A. D., Pushkarev, A. V., and Maslov, A. A., "Flight Testing of DBD Plasma Separation Control System," AIAA Paper 2008-373, January 2008.

[17]Perry, A. E. and Chong, M. S., "A Description of Eddying Motions and Flow Patterns Using Critical Point Concepts," *Annual Review of Fluid Mechanics*, Vol. 19, 1987, pp. 125–155.

[18]Mhitaryan, A. M., Phridland, V. Y., Boyarskii, G. N., and Kas'yanov, V. A., "Experimental Studies of an Influence of the Electrohydrodynamic Effect on Aerodynamic Characteristics of an Airfoil," *Some Problems of Aerodynamics and Electrodynamics*, Vol. 2, Kiev Institute of Civil Aviation Engineering, Kiev, Ukraine, 1966, in Russian.

[19]Malik, M., Weinstein, L., and Hussaini, M. Y., "Ion Wind Drag Reduction," AIAA Paper 83-0231, January 1983.

[20]Roth, J. R., Sherman, D. M., and Wilkinson, S. P., "Electrohydrodynamic Flow Control with a Glow-Discharge Surface Plasma," *AIAA Journal*, Vol. 38, No. 7, 2000, pp. 1166–1172.

Configuration	Dielectric Materials	Actuator Configuration
A	0.25 in Teflon	spanwise electrode
B	0.25 in Teflon	3 in finger electrodes
C	0.25 in Teflon, 0.014 in Kapton	3 in finger electrodes
D	0.02 in Kapton	2 in finger electrodes
E	0.25 in Teflon, 0.020 in Teflon/Kapton	3 in finger electrodes

Table 1. List of plasma actuators tested.

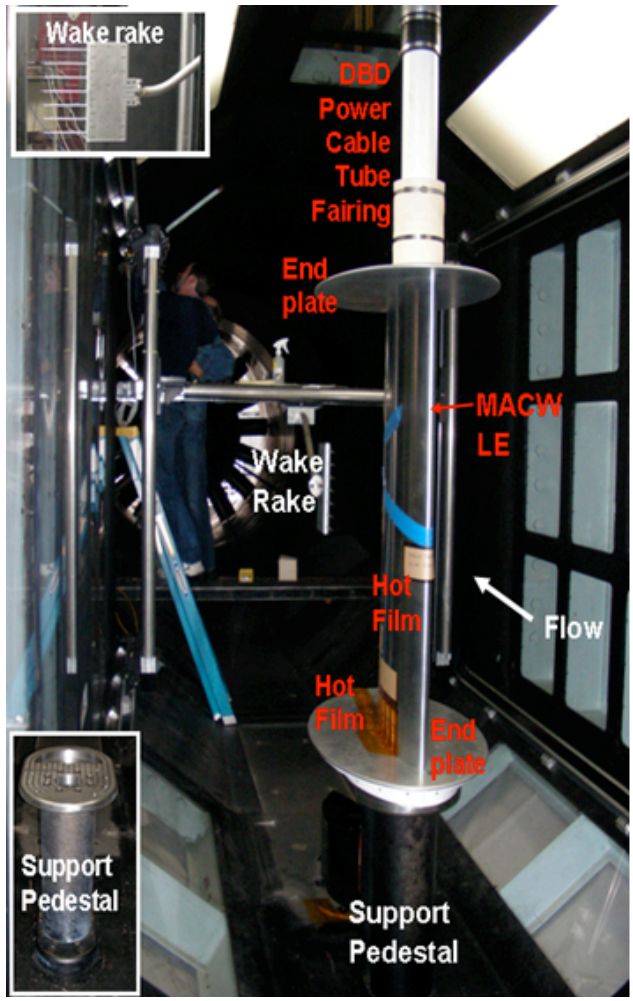

(a) Front view, looking downstream.

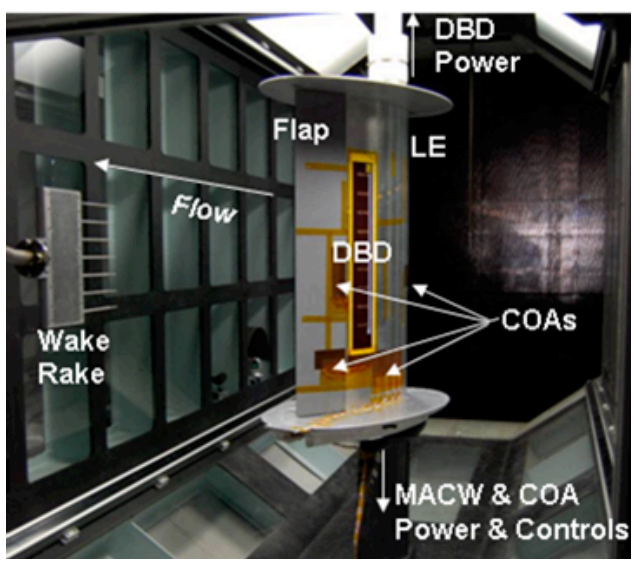

(b) Rear view, looking upstream.

Figure 1. Test article mounted in wind tunnel.

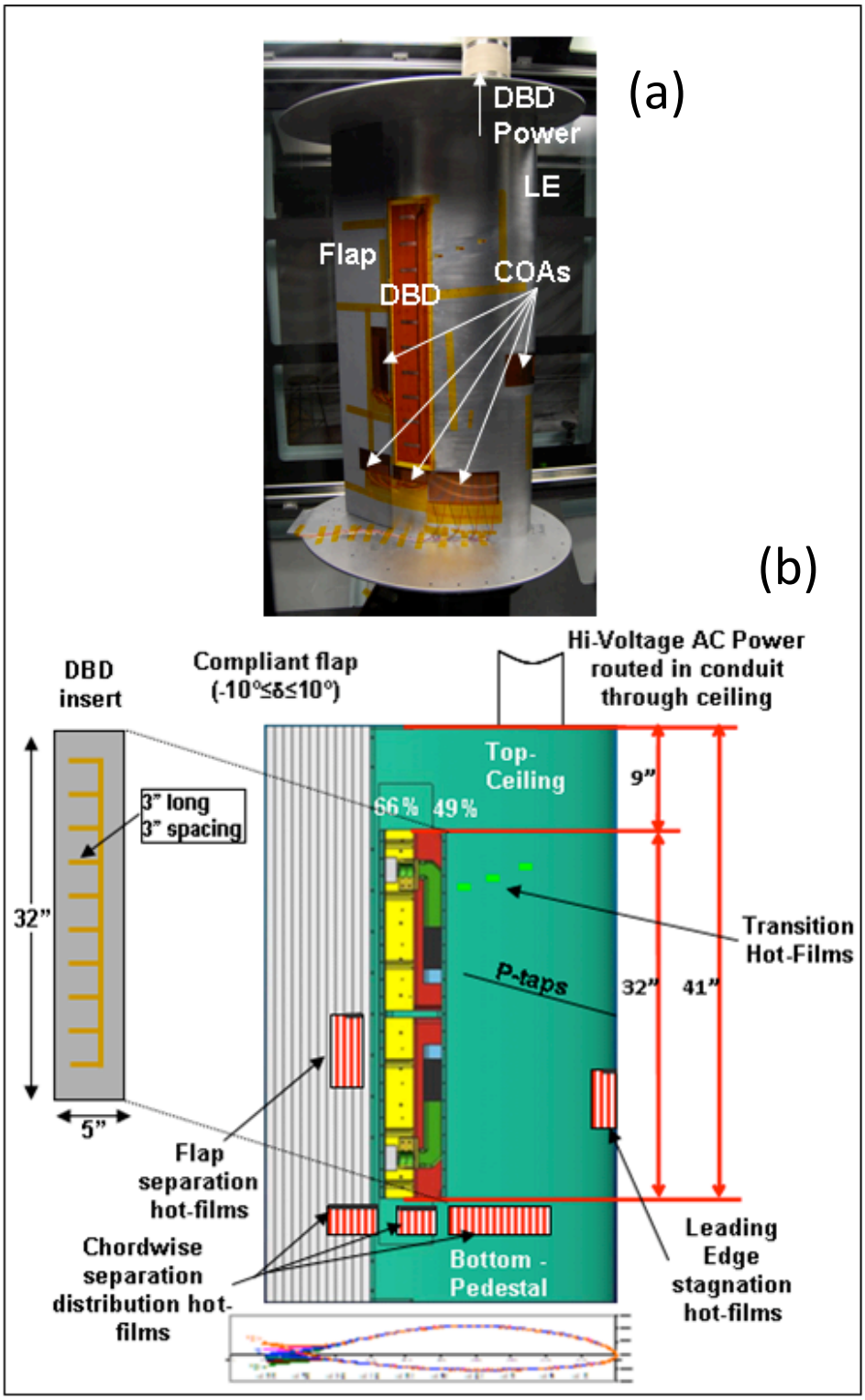

Figure 2. Instrumentation and plasma actuator installation. (a) View of suction-side of airfoil. (b) Schematic diagram of installation.

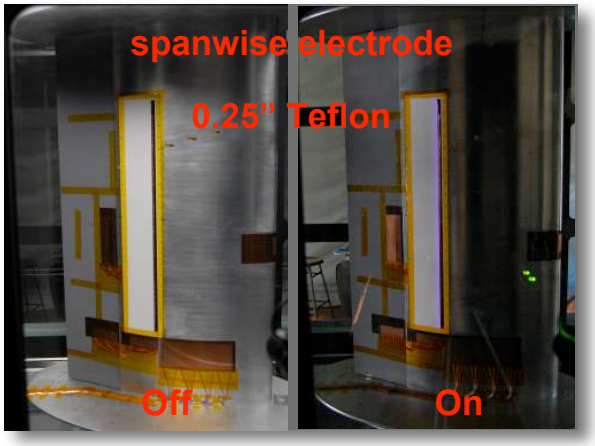

(a) Configuration A.

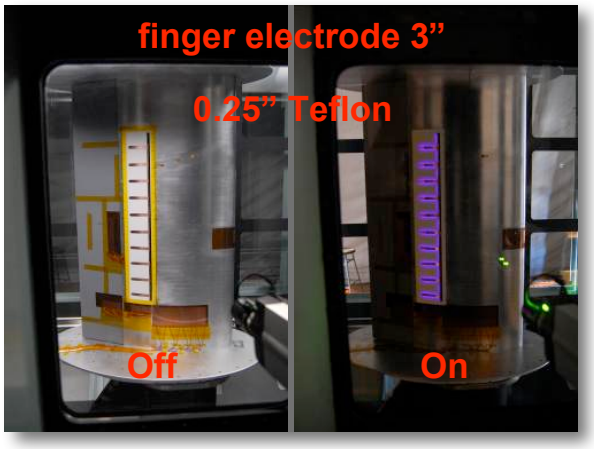

(b) Configuration B.

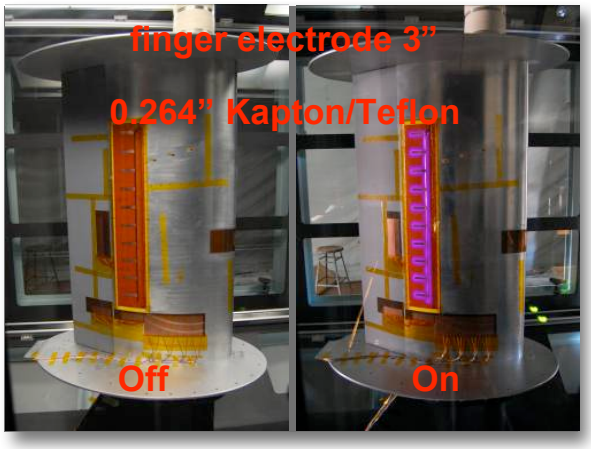

(c) Configuration C.

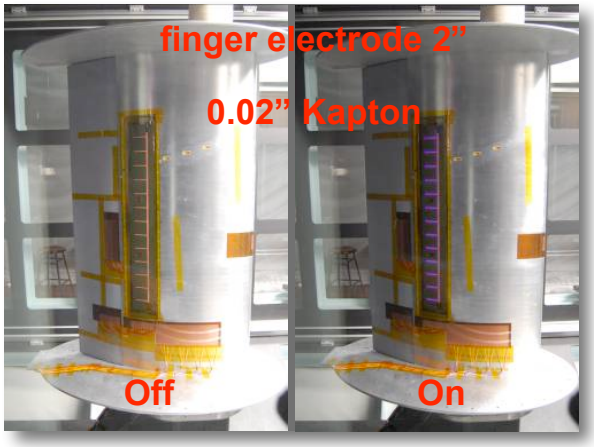

(d) Configuration D.

Figure 3. Plasma actuator designs. See Table 1 for description of actuator configurations.

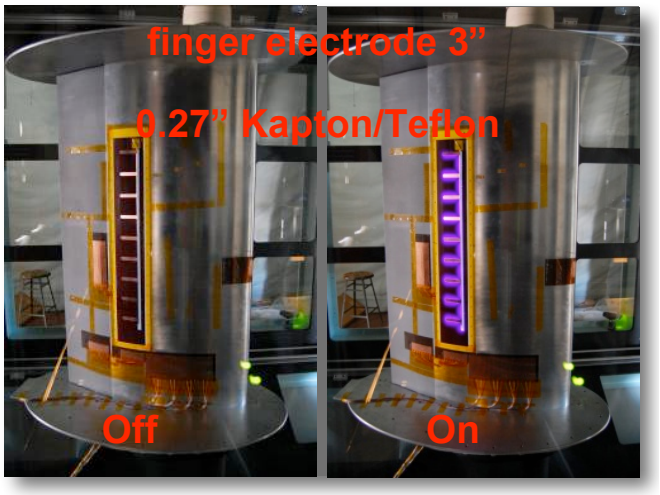

(a) Installation in tunnel.

(b) Close-up of glowing actuator.

Figure 4. Plasma actuator Configuration E. See Table 1 for description of actuator configurations.

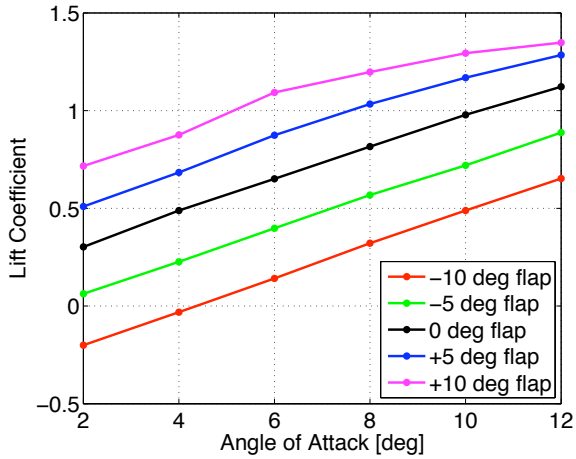

(a) Lift vs. angle-of-attack.

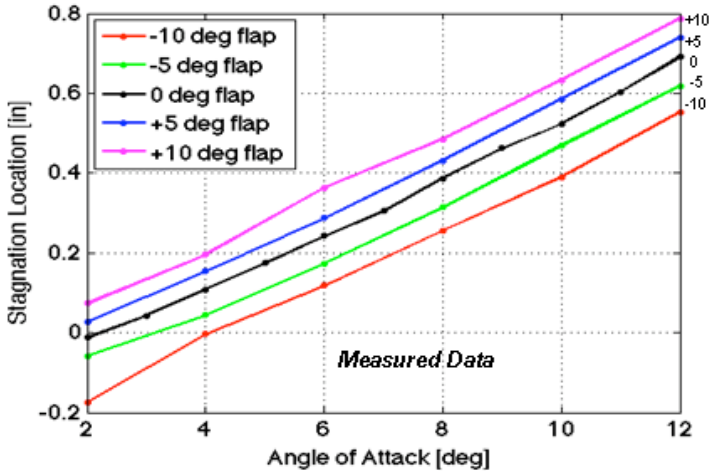

(b) Stagnation location vs. angle of attack.

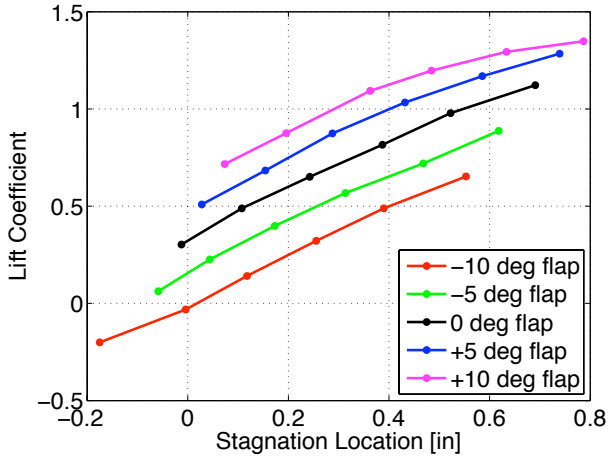

(c) Lift vs. stagnation location.

Figure 5. Hot-film measurements of leading-edge stagnation line location at Mach 0.05.

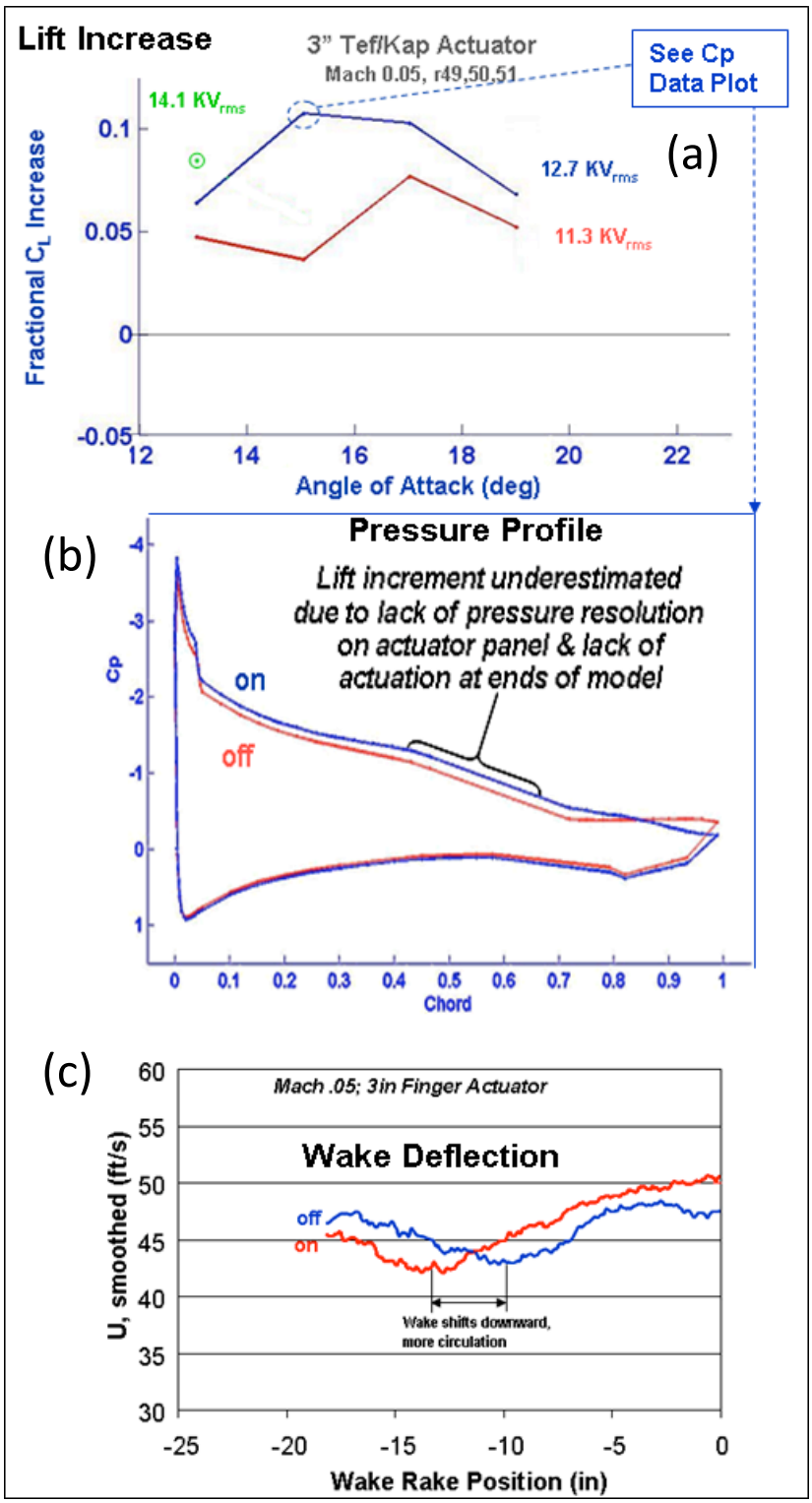

Figure 6. Effect of actuator Configuration C at Mach 0.05 with 10 deg flap deflection. (a) Lift change versus angle-of-attack and input voltage. (b) Pressure coefficient versus position (15 deg AoA, 12.7 kV$_{\rm rms}$ input). (c) Profile of streamwise velocity in airfoil wake (15 deg AoA, 12.7 kV$_{\rm rms}$ input, 1.5 chords downstream).

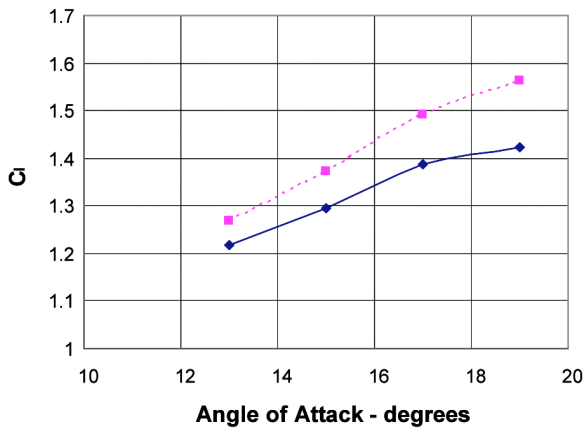

(a) Lift coefficient, Mach 0.05.

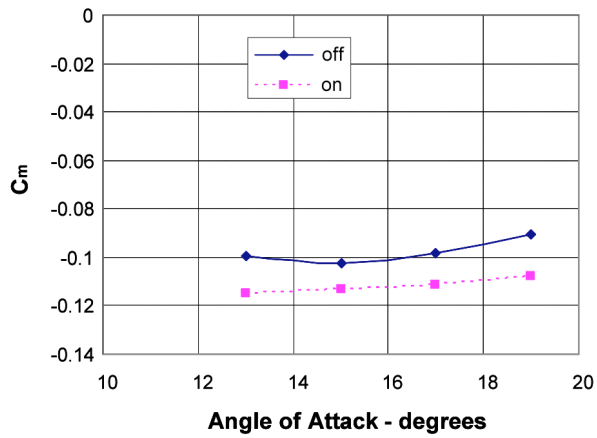

(b) Moment coefficient, Mach 0.05.

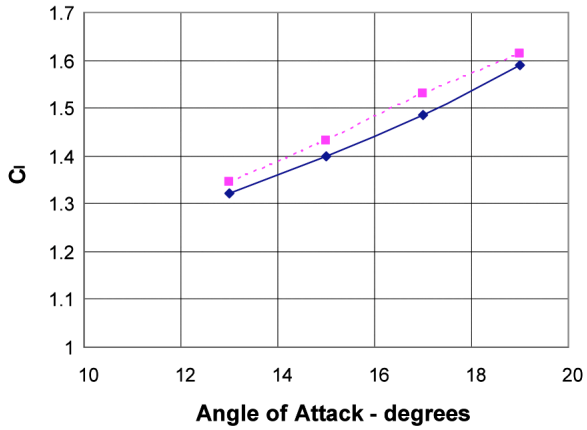

(c) Lift coefficient, Mach 0.10.

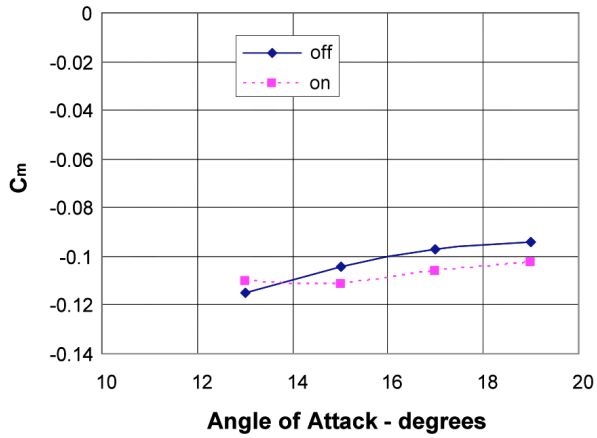

(d) Moment coefficient, Mach 0.10.

Figure 7. Effect of actuation on lift and moment coefficients (Configuration E, 12.7 kV$_{\mathrm{rms}}$ input, 10 deg flap deflection).

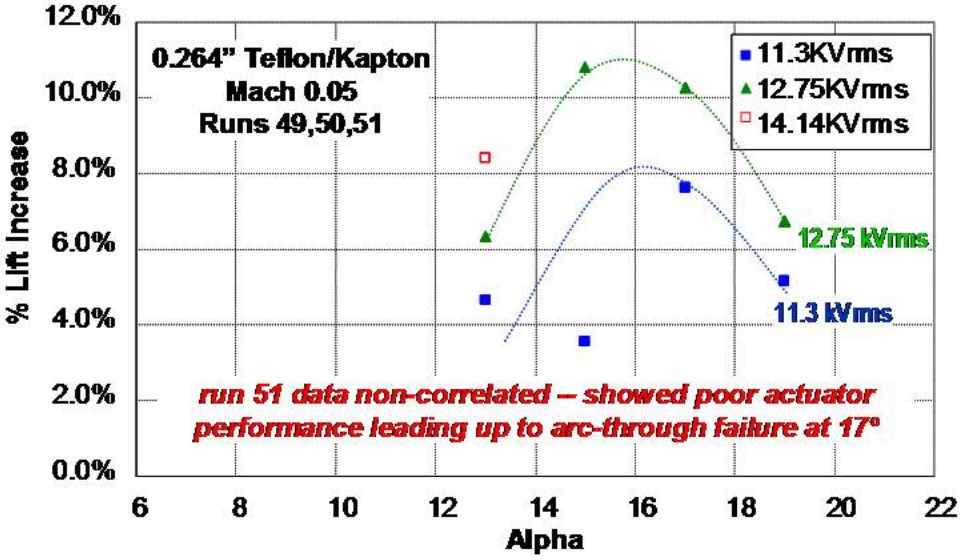

(a) Configuration C

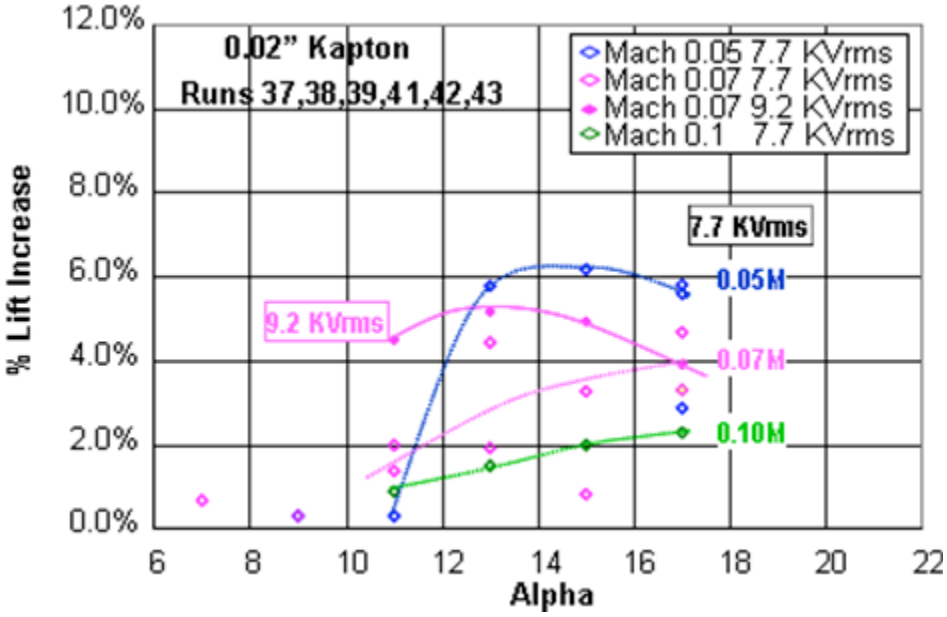

(b) Configuration D.

Figure 8. Effect of angle-of-attack, excitation voltage, and Mach number on lift change. Flap deflection 10 deg.

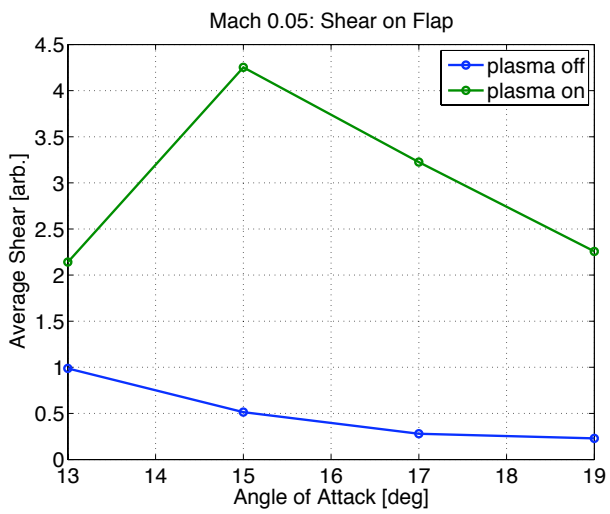

(a) Flap shear, 76.8% chord station on suction side, Mach 0.05.

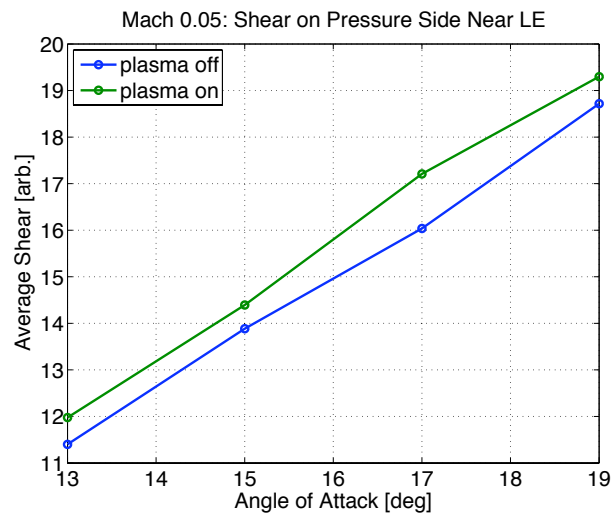

(b) Leading-edge shear, 0.17% chord station on pressure side, Mach 0.05.

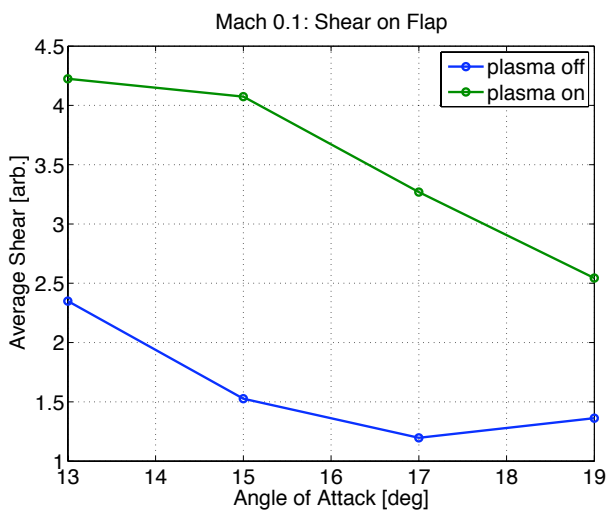

(c) Flap shear, 76.8% chord station on suction side, Mach 0.10.

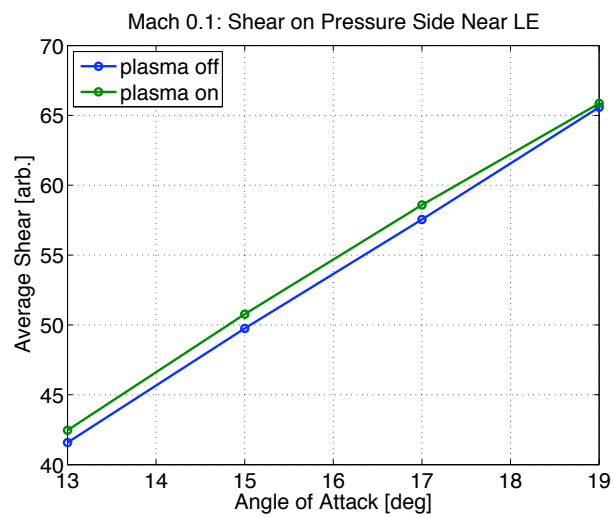

(d) Leading-edge shear, 0.17% chord station on pressure side, Mach 0.10.

Figure 9. Shear stress response to actuation, Configuration E. Flap deflection 10 deg.

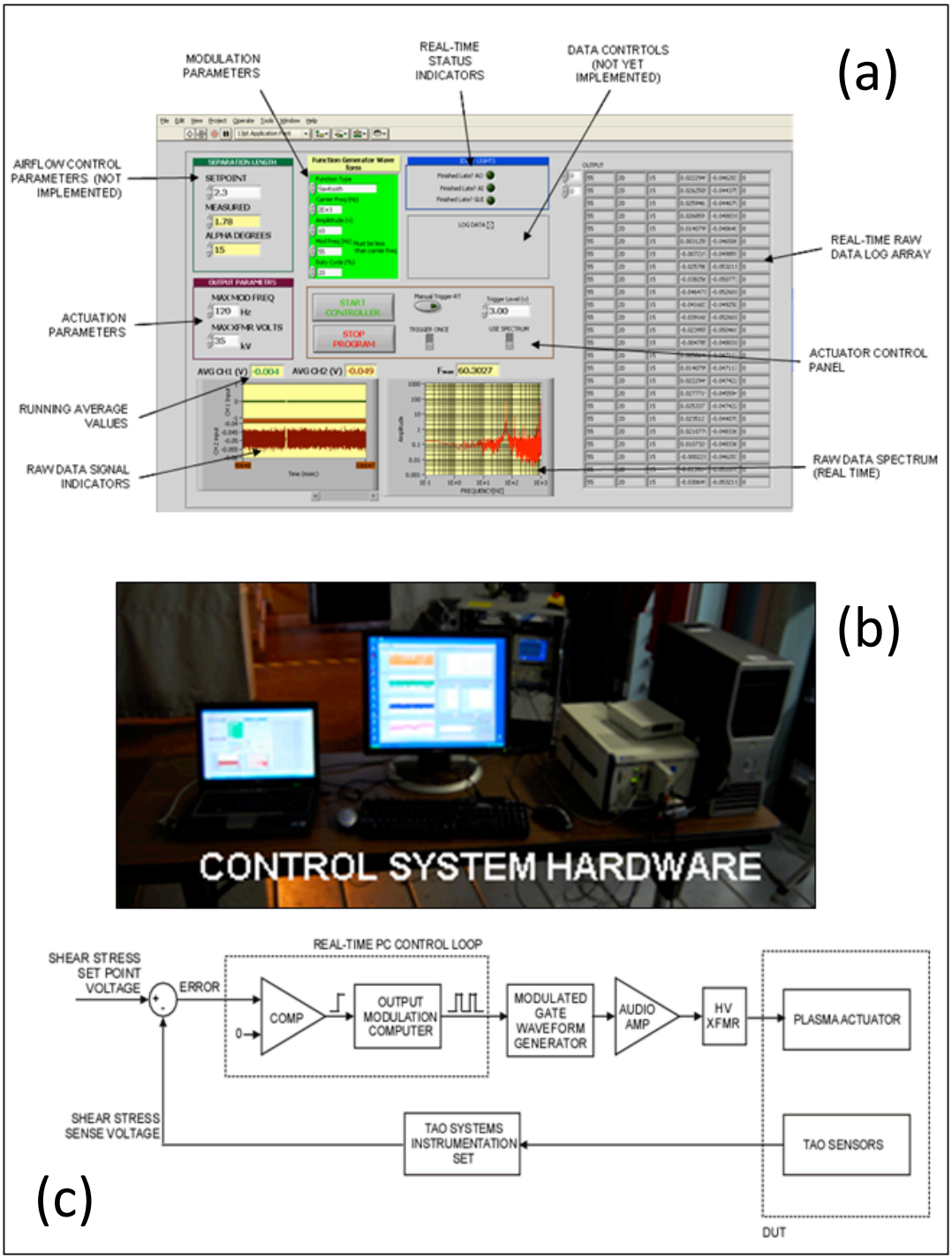

Figure 10. Closed-loop flow control system. (a) Control software. (b) Control hardware. (c) Flow chart.

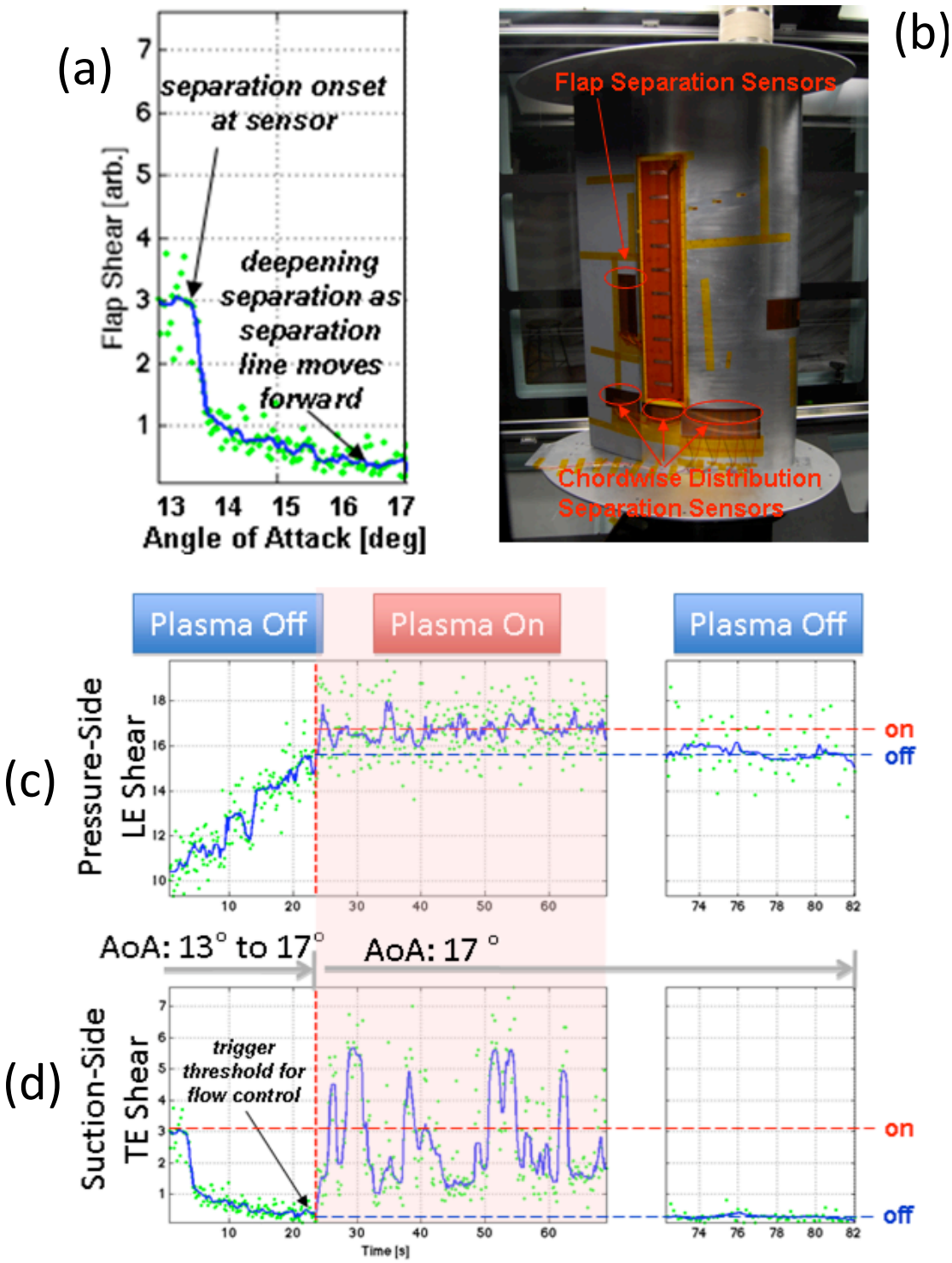

Figure 11. Closed loop flow control triggered by flap shear-stress measurements, Configuration E, flap deflection 10 deg. (a) Suction-side shear vs. angle of attack. (b) Sensor locations. (c) Pressure-side shear time-history (0.17% chord station). (d) Suction-side shear time-history (76.8% chord station).